

Supporting Information

Biomimetic Electro-oxidation of Alkyl Sulfides from Exfoliated Molybdenum Disulfide Nanosheets

*Lahcene Maachou,^{a†} Kun Qi,^{a†} Eddy Petit,^a Zhaodan Qin,^a Yang Zhang,^a Didier Cot,^a Valérie Flaud,^b Corine Reibel,^b Heba El-Maghrabi,^a Lei Li,^c Philippe Miele,^a Daniel Kaplan,^d Manish Chhowalla,^e Nicolas Onofrio,^f Damien Voiry^{*a}*

^a Institut Européen des Membranes, IEM, UMR 5635, University of Montpellier, ENSCM, CNRS, 34095 Montpellier Cedex5, France

^b Institut Charles Gerhardt, ICGM, UMR 5253, University of Montpellier, ENSCM, CNRS, 34095 Montpellier Cedex5, France

^c College of Biological, Chemical Sciences and Engineering, Jiaying University, Jiaying, Zhejiang 314001, China

^d US Army CCDC-AC RDECOM-ARDEC, Advanced Materials Technology Branch, Picatinny Arsenal, New Jersey 07806, USA

^e Department of Materials Science & Metallurgy, University of Cambridge, Cambridge, UK

^f Department of Applied Physics, The Hong Kong Polytechnic University, Hong Kong, China

*Correspondence to: damien.voiry@umontpellier.fr

[†] These authors contributed equally: L. Maachou, Dr. K. Qi

Table of Contents

Section Title

Pages

Chemicals and reagents.....	3
Materials synthesis.....	3
Physical characterizations.....	3
Electrocatalytic DMS oxidation in water.....	4
Preparation of the 20%Pt/C and Pd electrodes.....	4
Raman spectroscopy on the MoS ₂ electrodes.....	5
Estimation of the C _{dl} of 1T' MoS ₂ measured in water-based electrolyte.....	5
Estimation of the C _{dl} of Pt-NP (20%Pt/C) measured in organic electrolyte.....	7
Calibration of the Ag/AgNO ₃ reference electrode and potential window of the electrolyte.....	8
Cu underpotential deposition.....	10
Electrochemical impedance spectroscopy (EIS).....	10
Detection of the products of the reaction via Nuclear Magnetic Resonance (NMR).....	13
Physical characterization of the electrodes after 24 hours of operation.....	14
Calculation of the binding energy (E _b) of DMS.....	14
Preparation of amorphous MoS _x and defective MoS ₂ nanosheets.....	20
XPS analyses of amorphous MoS _x and defective MoS ₂ nanosheets.....	20
Evidence of radical formation during the oxidation of DMS under argon.....	21
Electron paramagnetic resonance measurements.....	21
Proposed mechanism for the electro-oxidation DMS.....	23
References.....	23
Author contributions.....	23

Experimental Procedures

Chemicals and reagents

Acetonitrile, MoS₂, tetraethylammonium tetrafluoroborate (NEt₄BF₄) n-butyllithium (1.6 M in hexane), and Bis[rhodium($\alpha,\alpha,\alpha',\alpha'$ -tetramethyl-1,3-benzenedipropionic acid)] (Rh₂(esp)₂) were purchased from Sigma Aldrich. 5% Nafion and 20% Pt/C was purchased from Alfa Aesar. Organic solvents were purchased from either Sigma Aldrich or Alfa Aesar and used as received. Ultra-high purity Argon was purchased from Airgas.

Materials synthesis

The 1T' MoS₂ electrodes were prepared from chemically exfoliated 1T' MoS₂ nanosheets. Chemically exfoliated MoS₂ nanosheets were obtained following our previously reported method based on lithium intercalation^[1]. Thin films of MoS₂ were prepared alternatively by drop-casting and controlled evaporation on 4 mm-diameter glassy carbon electrodes. The amount of deposited catalyst on the electrode is $\sim 60 \mu\text{g cm}^{-2}$.

The 2H MoS₂ electrodes were obtained by thermally annealing 1T' phase MoS₂ electrodes. The thermal annealing was performed at 300°C (ramping rate: 5°C/min) under vacuum with a 100 sccm 5% H₂/Ar flow for 60 minutes.

Physical characterizations

AFM images were obtained in Digital Instruments Nanoscope IV in tapping mode with cantilevers with spring constant of 40 N/m and tip curvature < 10 nm and a frequency of 325 kHz. Atomic force microscopy (AFM) was performed on the chemically exfoliated nanosheets. Sub-monolayer thin films were prepared by vacuum filtration using a nitrocellulose ester membrane with 25 nm pore size. The films were delaminated on the surface of deionized water and finally scooped directly on a SiO₂/Si wafer. X-ray photoelectron spectroscopy (XPS) measurements were performed with a Thermo Scientific K-Alpha spectrometer. All spectra were taken using an Al K α microfocused monochromatized source (1486.7 eV), a spot size of 400 μm and a 15eV pass energy. Raman spectra were obtained using a Renishaw 1000 system operating at 514 nm (2.41 eV).

Electrochemical tests

The electrochemical measurements were carried out using a 3-electrode cell with a 0.1 M tetraethylammonium tetrafluoroborate (NEt₄BF₄) in acetonitrile using a VSP potentiostat (Bio-Logic Science Instruments). The concentration of dimethyl sulfide was fixed to 0.1 M and the electrolyte solution was purged with argon for 30 min prior the measurements. An Ag/AgNO₃ (0.1 M AgNO₃) electrode in 0.1 M NEt₄BF₄ in acetonitrile and a platinum wire were used as reference and counter-electrode respectively. The reference electrode was calibrated using the well-known reduction oxidation signals of ferrocene: Fc (Figure S5). Potentials in the voltammograms are corrected to NHE using the equation: $E(\text{V vs. NHE}) = E(\text{V vs. Fc/Fc}^+) +$

630 mV [2]. We defined the onset potential as the potential (vs. RHE) at which the reaction begins and the Faradaic current starts to increase.

Prior any measurements, the MoS₂ and 20% Pt/C electrodes were cycled at least 40 times until giving stable responses. The double-layer charge capacitance (C_{dl}) was measured by cycling the electrodes at increasing from 5 mV s⁻¹ up to 200 mV s⁻¹ between 0 to 100 mV vs. Ag/AgNO₃. The C_{dl} for the different electrodes was estimated from the slope of the difference of current density at 50 mV vs. Ag/Ag NO₃.

Results and Discussion

Electrocatalytic DMS oxidation in water

The electrocatalytic activity of supported Pt-NP (20%Pt/C) and 1T' MoS₂ nanosheets toward the oxidation of DMS in water were measured using a 0.5 M Na₂SO₄ electrolyte solution. The concentration of DMS used in the experiments was 0.1 M. The electrochemical responses from both MoS₂ and Pt rapidly decreases between cycle #1 and #4 which can be explained by the degradation of the catalytic materials (Figure S1).

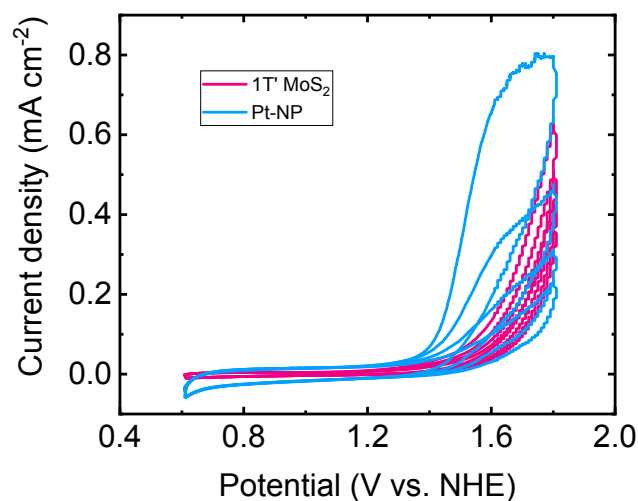


Figure S1. Cyclic voltammetry of 1T' MoS₂ and Pt-NP in a 0.5 M Na₂SO₄ electrolyte solution in presence of 0.1M of DMS.

Preparation of the 20%Pt/C and Pd electrodes

The 20%Pt/C electrodes were prepared by dispersing 20%Pt/C power (Alfa Aesar) at a concentration of 5mg mL⁻¹ in 2:1 isopropanol (IPA): water solution. Typically, 10 mg of 20%Pt/C was mixed with 1.8 mL of 2:1 IPA : water with 200 μ L of 5% Nafion solution (Alfa Aesar). The solution was drop-casted on a 4mm diameter glassy carbon electrode. The Pd

electrodes were prepared following the same procedure and using Pd particles (60 mesh, 99.95%).

Raman spectroscopy on the MoS₂ electrodes

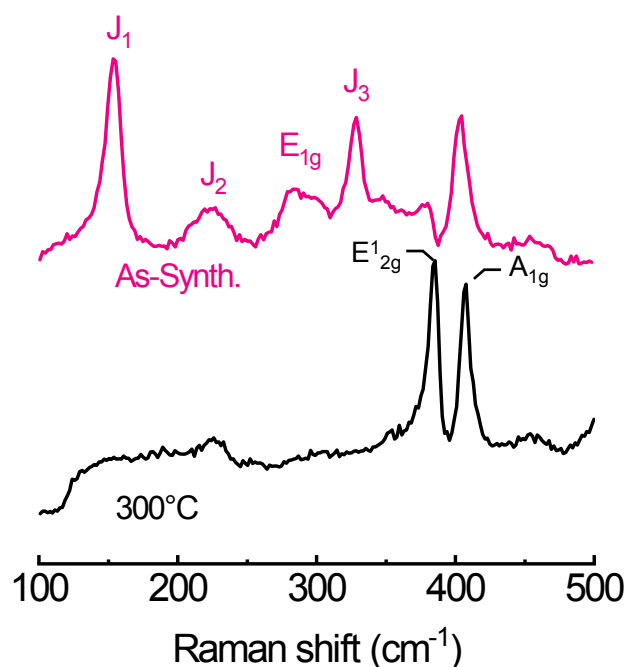


Figure S2. Raman spectroscopy on as-synthesized and 300°C annealed MoS₂ nanosheets. The signals from the 1T' polymorph (J₁, J₂, J₃) are visible on the Raman spectrum of as-synth. MoS₂. At the opposite, only the signatures from the 2H polymorph: E_{2g}¹ and A_{1g} are visible after 300°C annealing^[3].

Estimation of the C_{dl} of 1T' MoS₂ measured in water-based electrolyte

We compared the double-layer charge capacitance (C_{dl}) from 1T' MoS₂ electrodes measured in organic electrolyte (Figure 3) with the C_{dl} measured in water-based electrolyte (0.5 M H₂SO₄). The C_{dl} from MoS₂ in water-based electrolyte is found to ≈ 100-fold larger than in the case of organic electrolyte.

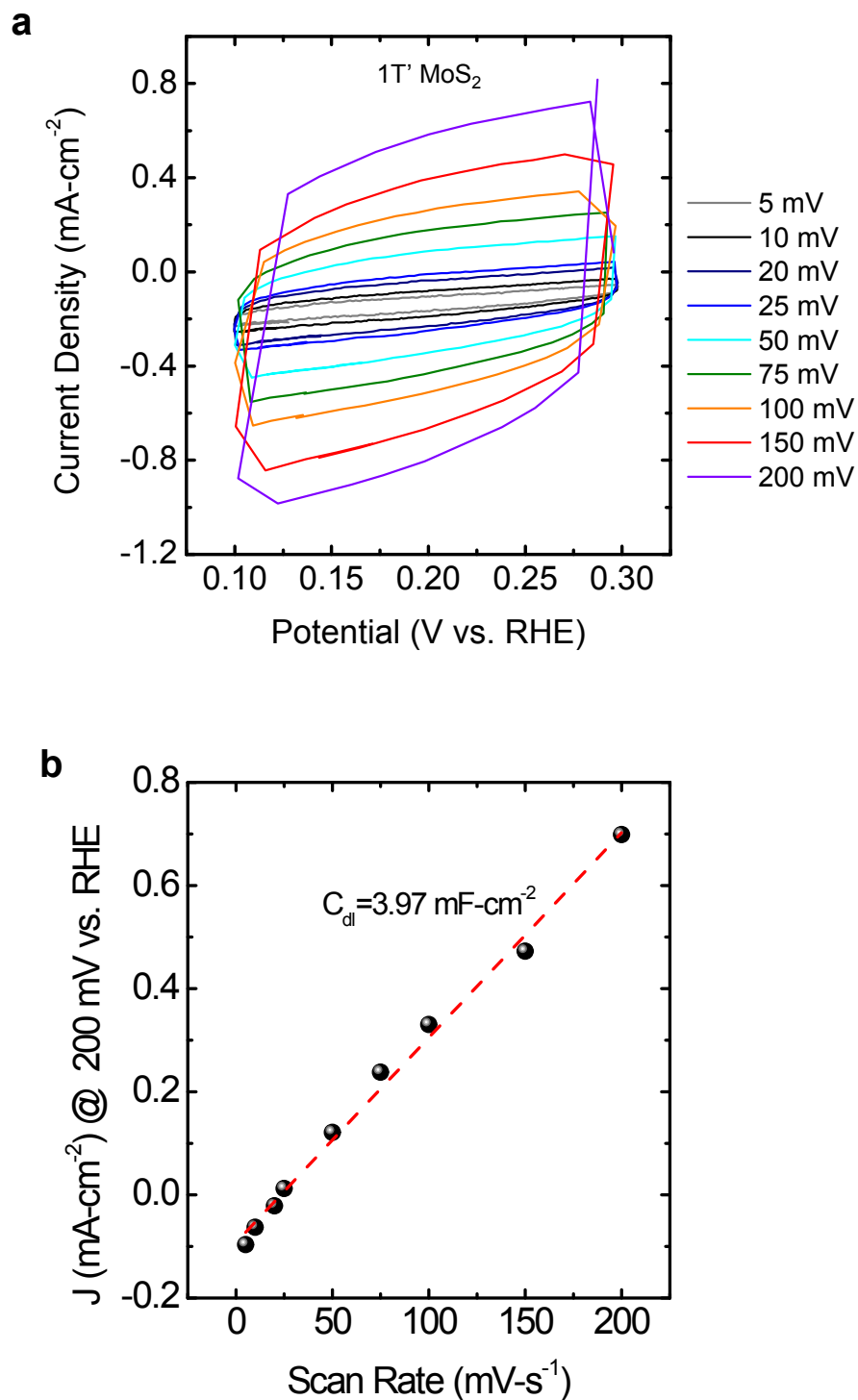


Figure S3. (a) Cycling voltammograms from MoS₂ electrodes in water- and organic-based electrolyte. (b) Evolution of $\Delta J_{200\text{mV}}$ with scan rate. The C_{dl} is equal to half of the slope obtained from the linear regression of $\Delta J_{200\text{mV}}$.

Estimation of the C_{dl} of Pt-NP (20%Pt/C) measured in organic electrolyte

We characterized the Pt-NP electrodes following the same methodology as for the 1T' and 2H phase. The C_{dl} values for 20% Pt/C is estimated to $2.9 \times 10^{-3} \text{ F cm}^{-2}$ much larger compare to the 1T' ($28.4 \times 10^{-5} \text{ F cm}^{-2}$) and 2H phase of MoS_2 nanosheets ($5.5 \times 10^{-5} \text{ F cm}^{-2}$) (Figure S4).

Such values of C_{dl} are attributed to the larger specific surface area of the passive carbon support.

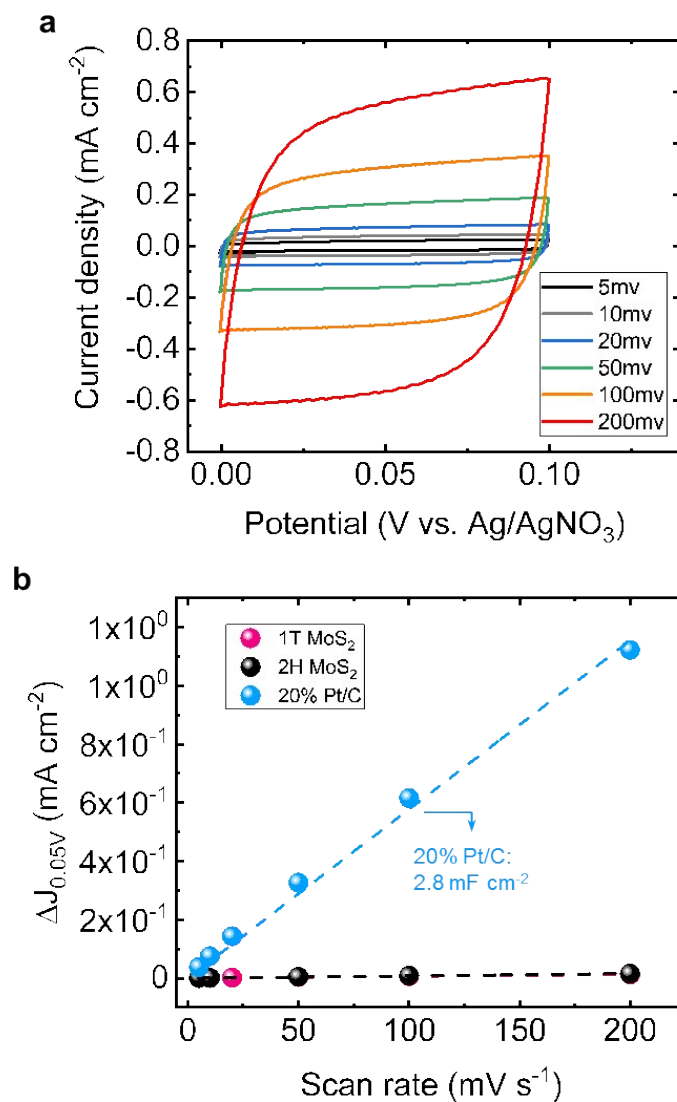


Figure S4. (a) Cycling voltammograms from Pt-NP electrodes measured in 0.1 M NET_4BF_4 in acetonitrile between 0 and 100 mV vs. Ag/AgNO_3 at increasing scan rates from 5 up to 200 mV s^{-1} . (b) Corresponding evolution of $\Delta J_{0.05V}$ with scan rates to extract the C_{dl} value.

Calibration of the Ag/AgNO₃ reference electrode and potential window of the electrolyte

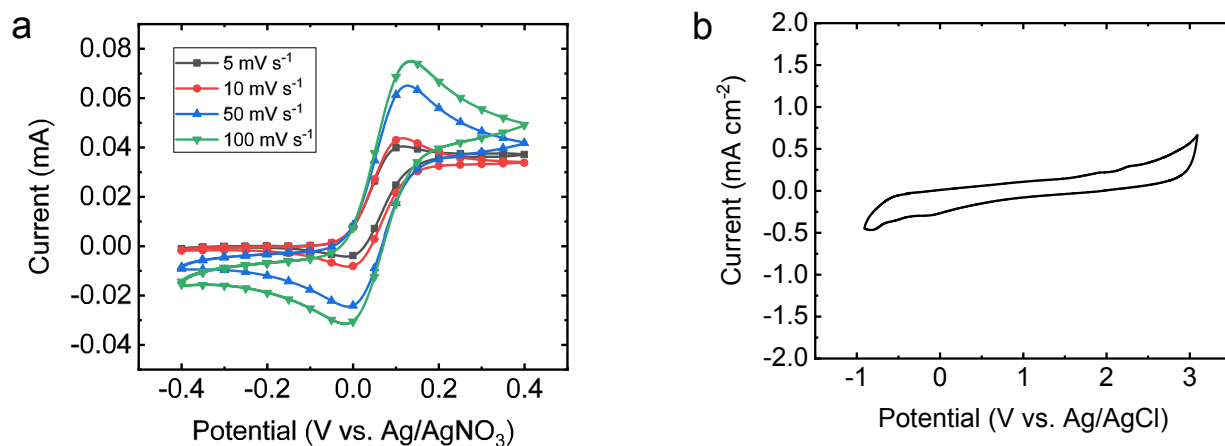


Figure S5. (a) Cyclic voltammetric (CV) responses a solution of 0.5 mM of ferrocene ($\text{Fe}(\text{C}_5\text{H}_5)_2$) in acetonitrile using a Ag/AgNO₃ (0.1 M) reference electrode in acetonitrile. We found that $E_{1/2}(\text{Fc}/\text{Fc}^+) = E_{\text{Ag}/\text{AgNO}_3} + 45 \text{ mV}$. (b) Cyclic voltammetry of a glassy carbon electrode in 0.1 M NEt₄BF₄ in acetonitrile.

Influence of the presence of DMS on the polarization curves

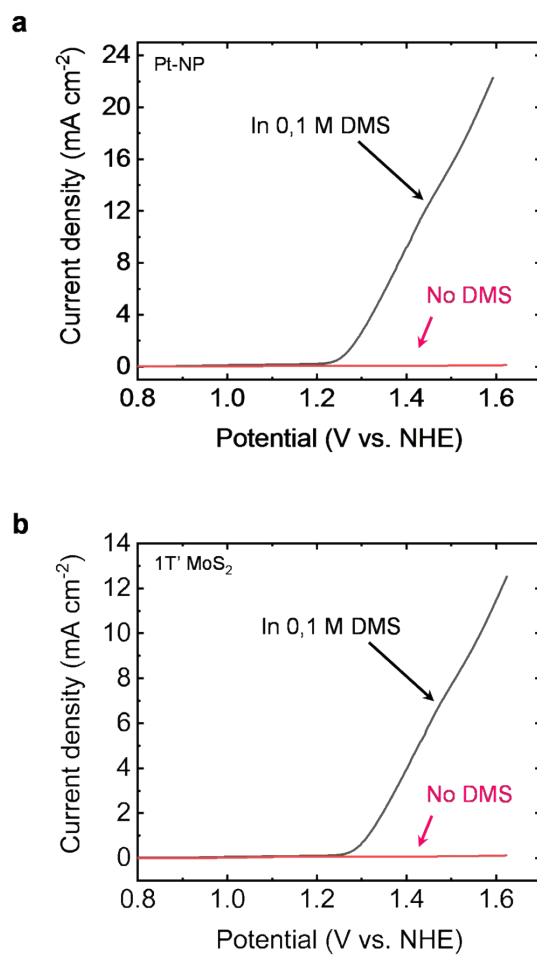
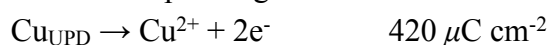


Figure S6. Polarization curves for 1T' MoS₂ (a) and Pt-NP (20%Pt/C) (b) in absence and in presence of 0.1 M DMS.

Cu Underpotential Deposition

Copper is an ideal metal for UPD on platinum because of the similarity of the atomic radii of the two metals Cu: 1.28 Å and Pt: 1.39 Å. We followed the same procedure as previously reported by Green and Kucernak^[4]. The UPD experiments were performed in a 0.1 mol L⁻¹ H₂SO₄ solution alone or with 2 mmol L⁻¹ of CuSO₄. First the 20%Pt/C electrodes were cleaned by pre-polarizing it at 1 V vs. RHE for 120 s to make sure that no copper was present on the surface of the Pt nanoparticles. The potential was then increased to 0.3 V vs. RHE for 100 s during which time a monolayer of copper can be deposited on platinum electrode surface. The potential was then swept at 10 mV s⁻¹ up to a potential of 1 V in order to strip off the deposited copper. The resulting Cu stripping peak charge was extracted and used to calculate the surface area assuming an adsorption ratio of a single Cu atom to each surface metal atom and an electrodeposition valency of +2 corresponding to^[4]:



Calculations of the surface areas of these electrodes were carried out by using EC-lab software (Bio-Logic Science Instruments) to calculate the UPD stripping charge of the current voltage curve, and using a conversion factor of 420 μC/cm².

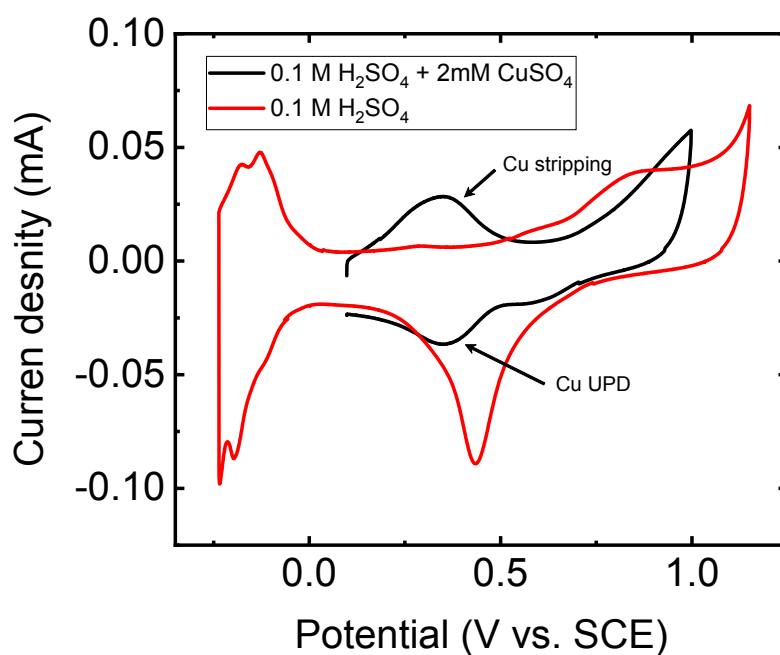


Figure S7. Cyclic voltammety responses from the Pt electrode in presence and absence of Cu²⁺. The stripping current measured after underpotential deposition of copper was measured by the integration of the peak area corresponding to the Cu stripping.

Electrochemical impedance spectroscopy (EIS)

The electrochemical impedance spectra have been recorded at 1300 and 1350 mV vs. NHE with an AC voltage of 5 mV from 10^6 to 0.01 Hz. The spectra have been fitted using the analogue circuit shown in Fig. S8c. R_S , R_{CT} , R_{CE-EL} refer to the series resistance, the charge transfer and the electrolyte resistance while C_{dl} and C_{CE-EL} refer to the double layer capacitance of the working electrode and the counter electrode/electrolyte. The values of the different EIS parameters are summarized in Table S1.

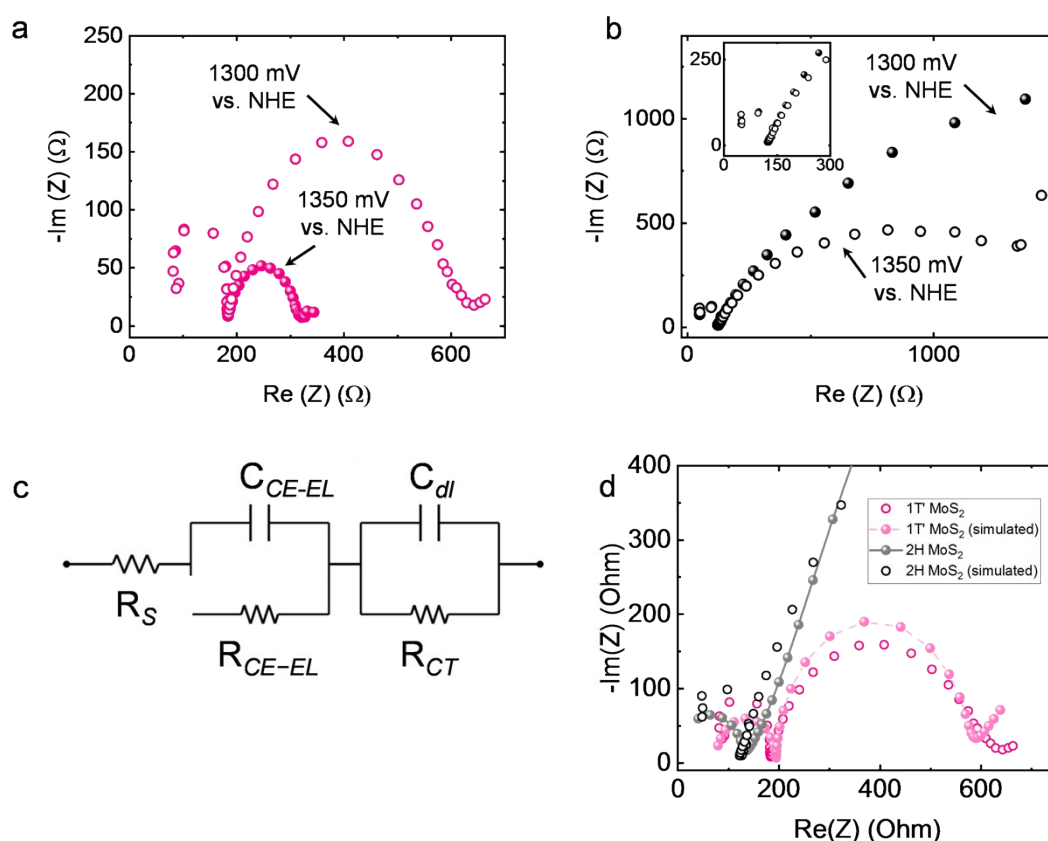


Figure S8. Nyquist impedance spectra for the 1T' (a) and 2H (b) phases of MoS₂ measured at an overpotential of 1300 mV and 1350 mV vs. NHE. (c) Equivalent electrical circuit used for fitting the EIS spectra. (d) Measured and simulated Nyquist impedance spectra for the 1T' and 2H phases of MoS₂ measured at an overpotential of 1300 mV vs. NHE.

Table S1. Impedance parameter measured at 1300 mV vs. NHE and 1350 mV vs. NHE for the 1T' and 2H phases of MoS₂ during the oxidation of DMS.

	$\eta= 1300$ mV 1T'	$\eta= 1350$ mV 1T'	$\eta= 1300$ mV 2H	$\eta= 1350$ mV 2H
R_S (Ω)	74.64	75.7	0.01	0.01
R_{CE-EL} (Ω)	119.4	117.9	135	124.8
R_{CT} (Ω)	374	117	6000	1478
C_{CE-EL} (F)	8.6×10^{-6}	8.31×10^{-6}	3.71×10^{-6}	8.1×10^{-6}
C_{dl} (F)	6.5×10^{-9}	6.56×10^{-8}	1.84×10^{-9}	1.9×10^{-12}

Detection of the products of the reaction via Nuclear Magnetic Resonance (NMR)

The identification of the products for the reaction was carried after the electrochemical reaction using ^1H NMR Nuclear Magnetic Resonance (NMR). The electrochemical reactions were performed by holding the potential at 1500 mV vs. NHE over 8 hours. 1 mL aliquots of the electrolyte solution were taken from the electrochemical cell after 4 hours and 8 hours of reaction. The aliquots were then diluted 100 times in d-acetonitrile for the NMR measurements.

The quantification of the DMSO in the electrolyte was estimated from the calibration curves of the NMR signals from DMSO. The calibration curves were obtained from measuring NMR spectra of the electrolyte solution with known concentrations of DMSO (Figure S9).

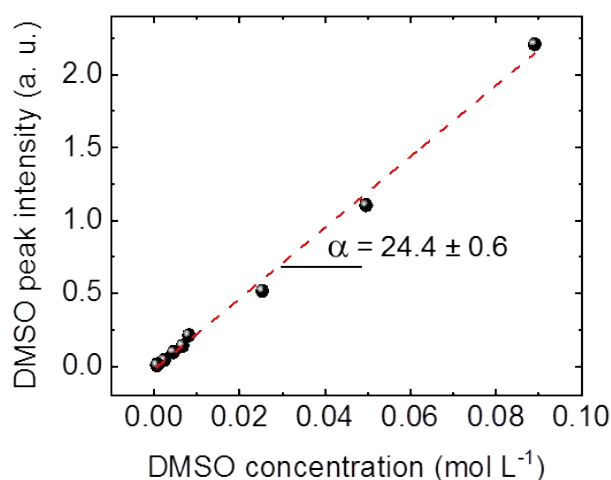


Figure S9. Calibration curve for the DMSO NMR signature.

To confirm the absence of dimethyl sulfone, we compared our results to reference samples (Fig. S10). The peak from dimethyl sulfone is detected at 2.91 ppm in the reference solution. No signals are detected even after 24 hours of reaction confirming the high selectivity of the reaction.

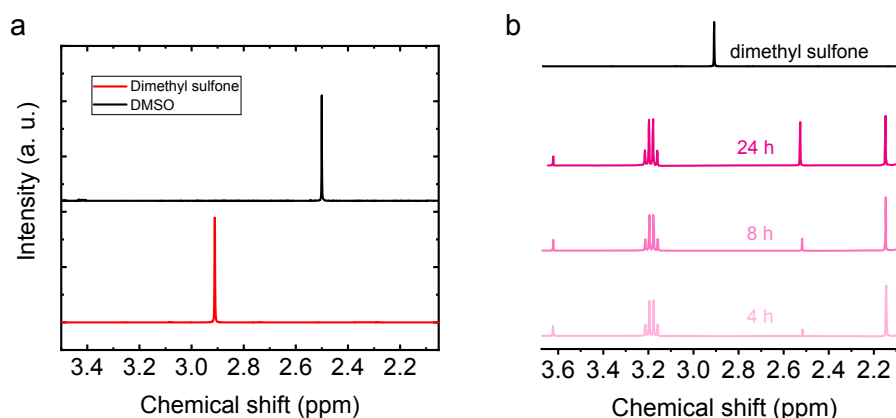


Figure S10. (a) NMR spectra of dimethyl sulfoxide and dimethyl sulfone. (b) NMR spectra of the electrolyte after 4, 8 and 24 hours of reaction at 1500 mV vs. NHE compared to the dimethyl sulfoxide reference.

Physical characterization of the electrodes after 24 hours of operation

To verify the stability of the electrode, we performed XPS and Raman spectroscopy on the electrode after 24 hours of operation at 1500 mV vs. NHE. According to XPS, virtually no signals from Mo^{6+} (Mo-ox) and oxidized S (S-ox) can be detected after electrocatalysis suggesting that the oxidation reaction of DMS does not lead to dramatic oxidation of MoS_2 (Fig. S11a,b). The Raman signatures for the 1T' phase are also preserved after the reaction as shown by the clear J_1 , and J_3 peaks at 149 cm^{-1} and 336 cm^{-1} as well as the E_{1g} peak at 281 cm^{-1} (Fig. S11c). These peaks are in perfect agreement with the predicted vibration mode for the 1T' phase of MoS_2 ^[5].

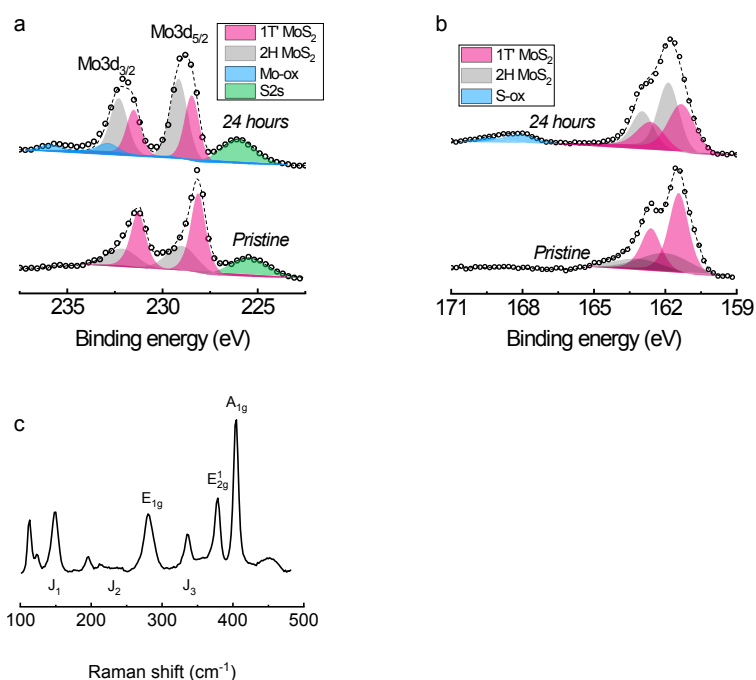


Figure S11. X-ray photoelectron spectroscopy of the Mo3d (a) and S2p (b) regions of 1T' MoS_2 after 24h of DMS oxidation reaction. (c) Raman spectrum of the 1T' MoS_2 nanosheets after 24 h of reaction.

Calculation of the binding energy (E_b) of DMS

Density functional theory (DFT) calculations were performed with VASP^[6,7] within the generalized gradient approximation proposed by Perdew, Burke, and Ernzerhof^[8]. We used Grimme's DFT-D2 method^[9] to correct for the van der Waals interaction poorly described by standard DFT. We studied the energetics of adsorbed DMS on monolayer H (octahedral) and T' (distorted octahedral) MoS_2 and, 6 atomic layers of Pt(111) with various coverage by varying the size of the supercells containing a single molecule of DMS. Supercells for MoS_2 and Pt

surfaces are represented Figure S12. An empty space of approximately 15 Å was systematically added in the z-direction to create the open surface.

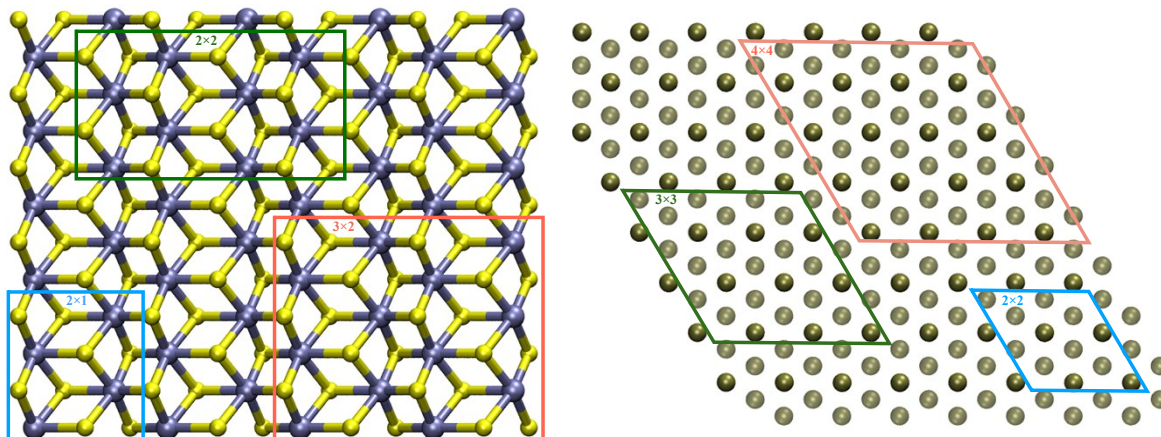


Figure S12. Surface supercell adopted for the adsorption coverage of MoS₂ (left) and Pt(111) (right).

For all DFT calculations, we used a kinetic energy cutoff of 400 eV and various k-meshes with approximately 40 k-points/lattice direction. Convergence was achieved when energy and forces reached a minimum value of 1×10^{-6} eV and 1×10^{-2} eV/Å, respectively. To find the most favorable location of adsorbed DMS on MoS₂ (and Pt) surface, we initially deposited the DMS molecule with the S-atom right above common adsorption sites of the surfaces and compared final structures, after geometry optimization. We found that DMS preferentially sits on top of a hollow site of MoS₂ and directly above a Pt atom. Figure S13 shows atomic structures of DMS adsorbed on the terrace sites of pristine and defective (with one S vacancy) 2H and 1T' phases of MoS₂. We define the coverage fraction as the number of hollow sites (i.e. the number of S atoms of the bottom layer) and first layer of Pt atoms in the supercell of MoS₂ and Pt slabs, respectively. The binding energy E_b was computed as:

$$E_b = E_{\text{DMS@slab}} - E_{\text{slab}} - E_{\text{DMS}}$$

with E_{DMS} , E_{slab} and $E_{\text{DMS@slab}}$ the energy of DMS, the MoS₂ (or Pt) slab and that of DMS adsorbed on MoS₂ (or Pt) slab. Following this definition, lower binding energy implies more favorable adsorption. The binding energies are reported Table S2.

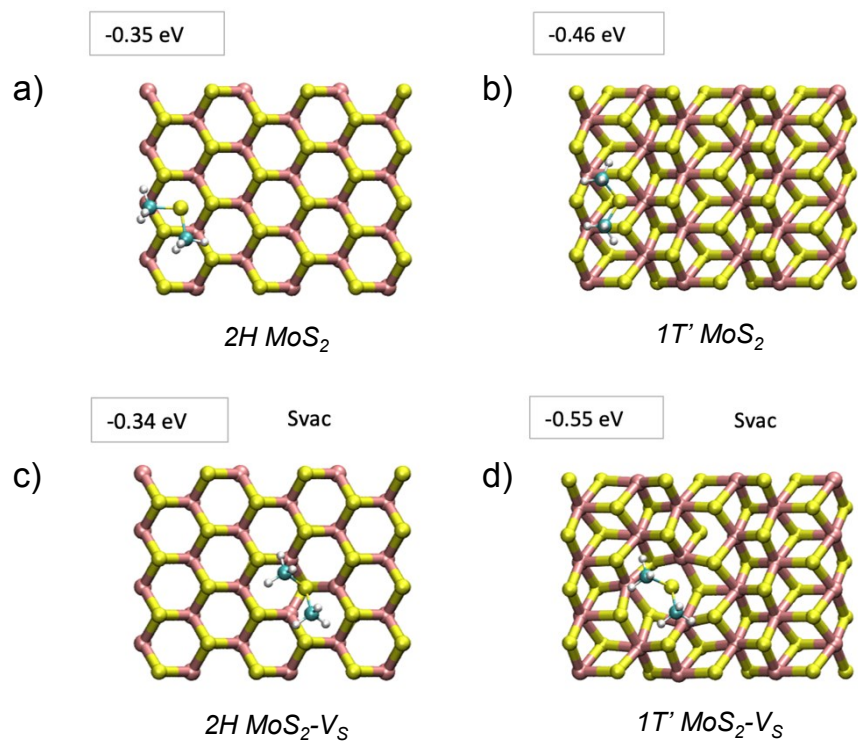


Figure S13. Unit cells of pristine (defect-free) and defect-rich of the 2H MoS₂ and 1T' MoS₂ used for the binding energy calculations.

Table S2. Supercell dimension, coverage percentage and binding energy corresponding to DMS adsorbed on defect-free and defect-rich MoS₂ and Pt surfaces.

	Supercell	Coverage %	Binding energy (eV)	Slab-DMS (Å)
DMS@2H MoS ₂ (terrace)	2×1	25	-0.29	2.9 (H-S)
	2×2	12.5	-0.31	
	3×2	8	-0.33	
	4×3	4	-0.35	
DMS@2H MoS ₂ (Mo 100%S-edge)			-0.89 ± 0.03	
DMS@1T' MoS ₂ (terrace)	2×1	25	-0.36	3.1 (H-S)
	2×2	12.5	-0.40	
	3×2	8	-0.45	
	4×3	4	-0.46	
DMS@1T' MoS ₂ (Mo100%S-edge)			-0.54 ± 0.04	
DMS@2H MoS ₂ -V _S (terrace)	4×3	4	-0.34	
DMS@1T' MoS ₂ -V _S (terrace)	4×3	4	-0.55	
DMS@Pt(111)	2×2	25	-2.01	2.3 (S-Pt)
	3×2	11	-2.40	
	4×3	6	-2.56	

Table S3. Bader charge on the atoms of DMS in vacuum, adsorbed on MoS₂ and on Pt. The sum of the partial charges on DMS gives the total charge transfer. A negative number indicates transfer from DMS to the surface and a positive number from the surface to DMS.

	DMS	DMS@MoS ₂	DMS@Pt111
C	-0.294	-0.306	-0.21
C	-0.301	-0.305	-0.208
H	0.102	0.114	0.035
H	0.06	0.073	0.128
H	0.12	0.134	0.139
H	0.089	0.107	0.037
H	0.095	0.109	0.133
H	0.139	0.154	0.133
S	-0.01	0.097	0.194
Charge transfer		0.177	0.381

Bader charges were calculated with the algorithm described in Ref. [10] and we define the charge density difference as $\Delta\rho = \rho_{AB} - \rho_A - \rho_B$ with ρ_{AB} , ρ_A and ρ_B : the charge density of the surface+DMS system, the surface, and the DMS molecule, respectively.

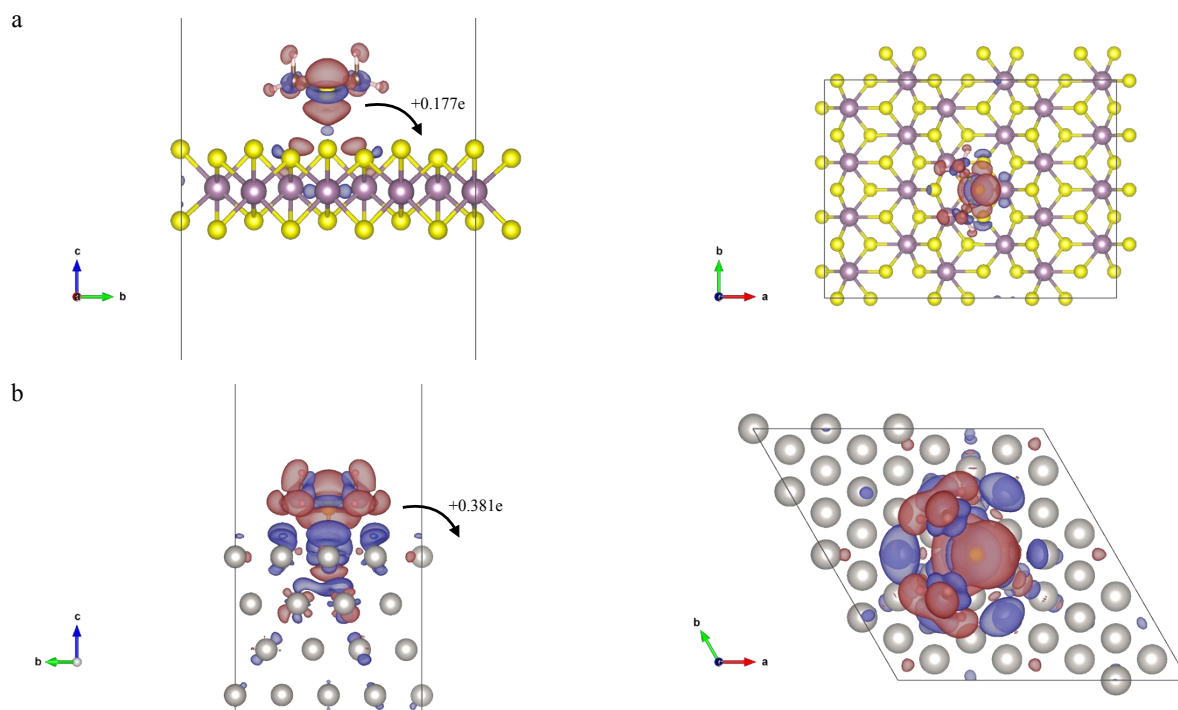


Figure S14. Charge density difference of DMS adsorbed on MoS₂ (a) and on Pt111 (b). Blue and red colors correspond to charge accumulation and depletion, respectively.

We also studied the adsorption of DMS at the edges of 2H and 1T' MoS₂. We considered the adsorption of DMS at sulfur ending edges by chopping the monolayer along the S row. To find the most favorable adsorption site, we computed a series of geometry optimization by randomly (random position in space and random rotations along x, y and z axis) approaching DMS to the edge leading to a distribution of binding energies, as reported Table S2. These distributions correspond to 4 and 8 stable configurations for 2H and 1T' edges, respectively. An example of the atomic structure of DMS at the edge of 2H and 1T' edges is reported Figure S15.

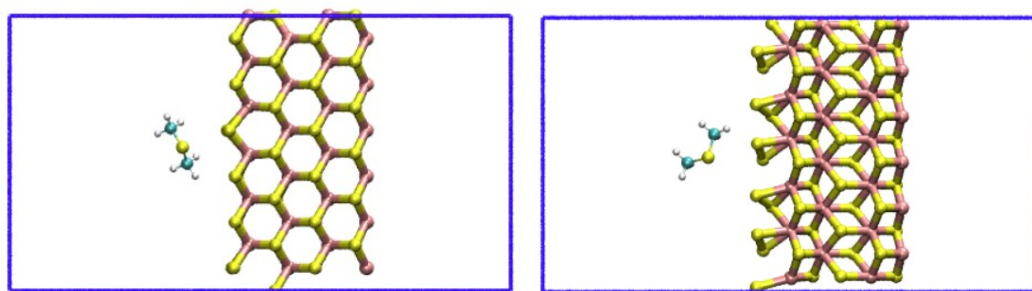


Figure S15. Configurations of DMS adsorbed at the S-edges of H and T' of MoS₂ strips. The binding energies over several configurations have been averaged and reported Table S2.

Preparation of amorphous MoS_x and defective MoS₂ nanosheets

Amorphous MoS_x (A-MoS_x)

A-MoS_x was synthesized following our previously reported method^[11]. 20 mg of (NH₄)₂MoS₄ was dispersed in 35 ml of DMF followed by sonication for 10 min at room temperature. The homogeneous, red-brown solution was then transferred into a 50 mL Teflon-lined autoclave. After 36 hours at 210°C, the product was collected by centrifugation and washed with ethanol. The A-MoS_x electrode were prepared following the same methodology as for the 1T' phase.

Defective MoS₂ nanosheets

Sulfur vacancies were generated in the MoS₂ nanosheets by thermally annealing under hydrogen (5% in argon, Varygon®) under vacuum 600 °C and 700 °C for 1 hour with a 10 °C min⁻¹ ramping rate. The obtained electrodes were denoted as MoS₂-V_S (annealed at 600 °C) and MoS₂-S_S (annealed at 700 °C)

Table S4 summarized the double layer capacitance for A-MoS_x, MoS₂-S_S and MoS₂-V_S electrodes in 0.1 M NEt₄BF₄ in acetonitrile

Table S4. Cdl of the different MoS_x electrodes in 0.1 M NEt₄BF₄ in acetonitrile.

	C _{dl} (μF cm ⁻²)
1T' MoS ₂	284
2H MoS ₂	55
A-MoS ₂	691
MoS ₂ -S _S	395
MoS ₂ -V _S	96

XPS analyses of amorphous MoS_x and defective MoS₂ nanosheets

The chemical structure of A-MoS_x and defective MoS₂ samples was analyzed using XPS (Fig. S14). The S:Mo ratios for the MoS₂ reach 0.63 and 1.79 corresponding to point-defect vacancies (V_S) and S-stripping (S_S) domains according to our previous study^[11]. At large density of vacancies, the stripping of S atoms is accompanied with the formation of under-coordinated Mo: MoS_x. For comparison the S:Mo ratio 2H MoS₂ is estimated to be 2.02.

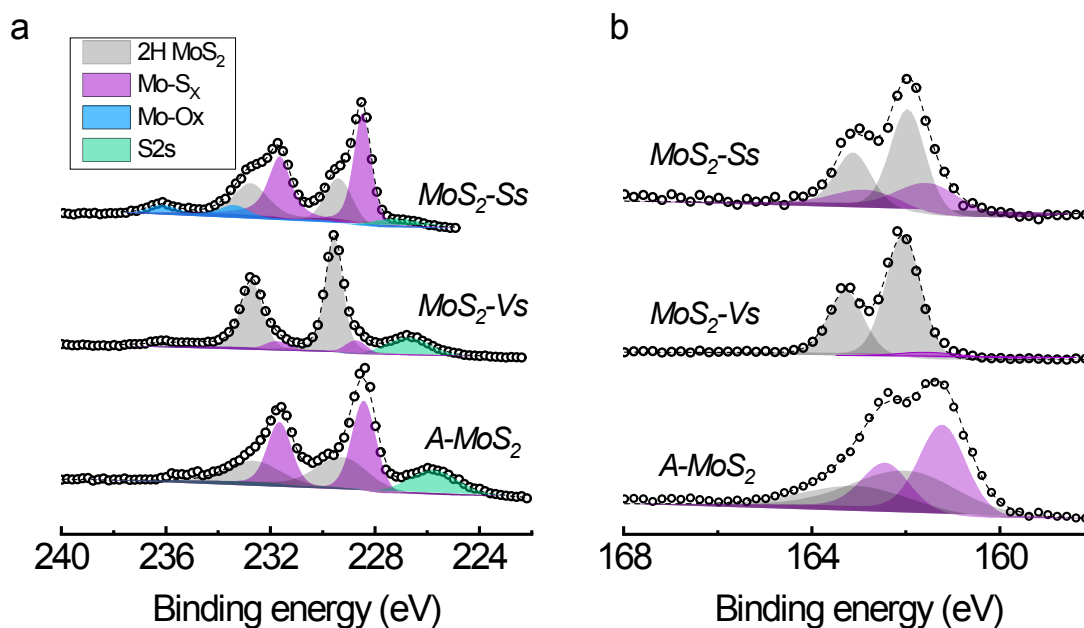


Figure S16. X-ray photoelectron spectroscopy of the Mo3d regions and S2p of amorphous MoS₂ (A-MoS_x) and defective MoS₂ with low and high concentration of defects: MoS₂-Vs and MoS₂-Ss. Component from the 2H phase and the undercoordinated Mo-S_x are shown in gray and purple respectively.

Evidence of radical formation during the oxidation of DMS under argon



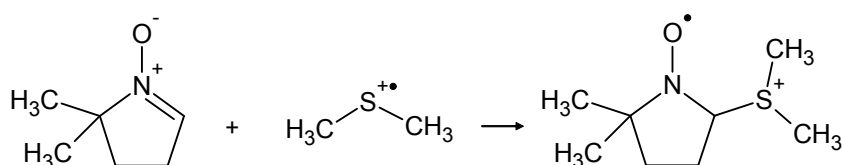
Figure S17. Photographic pictures of the electrochemical cells taken during the DMS oxidation performed under argon (a) and O₂ (b). No coloration of the solution is observed under oxygen due to the fast reaction between sulfur radicals and the oxygen molecules.

Electron Paramagnetic Resonance measurements

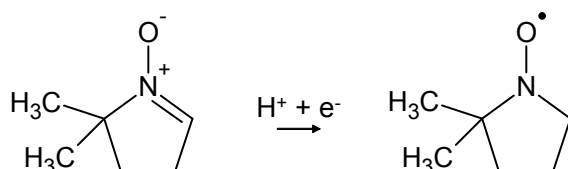
The electron paramagnetic resonance (EPR) spectra were collected at room temperature using a Bruker RPE Elexsys E500 spectrometer with X band (around 9.8 GHz) and in CW continuous

wave spectrometer, equipped with a ER4122 SHQ cavity. Spectra were recorded with a frequency of 100kHz, a modulation amplitude of 3G, and a microwave power of 20mW. A 0.1 M NEt_4BF_4 acetonitrile solution with 0.1 M DMS was used as electrolyte. 50 mg of 5,5-dimethyl-1-pyrroline N-oxide (DMPO, Sigma Aldrich, ESR grade) were dissolved in 15 mL of the electrolyte solution (equiv. to 30 mM) and the solution was purged with argon for 30 min prior the measurements. The potential of the working electrodes was hold at 1500 mV vs. NHE for 2h. 1 mL aliquots of the solution were collected at 30 min, 1h and 2h, transferred into capillaries and immediately analyzed by EPR. Blank experiments were performed under the identical condition in absence of DMPO.

The EPR spectrum can be decomposed into a combination of a 6-line and a 9-line signals for the trapping of the sulfur radical cations (*Equation 1*) and the reduction of the DMPO product (*Equation 2*) at the cathode. The signals are indicated by red and black arrows in Figure S16.



(Equation 1)



(Equation 2)

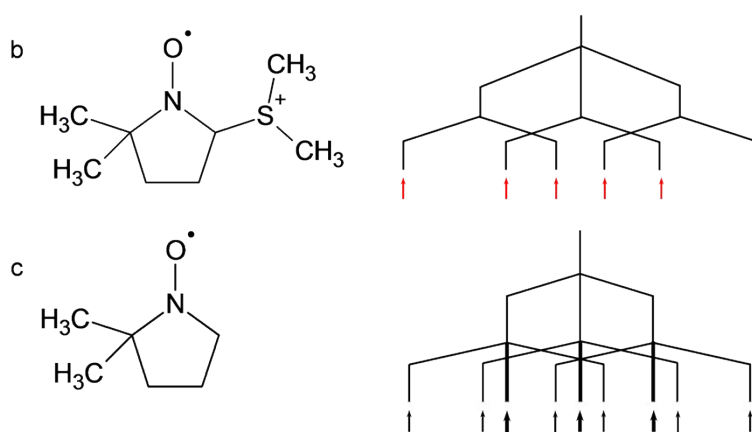
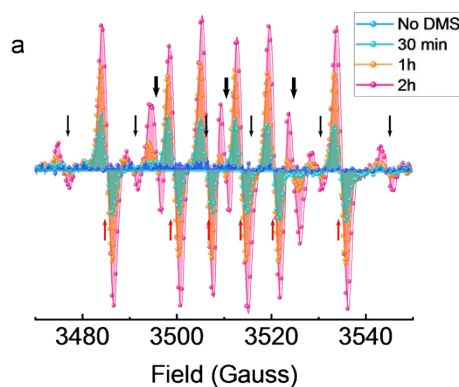


Figure S18. Interpretations of the EPR spectra presented in Fig. 8a.

Proposed mechanism for the electro-oxidation DMS

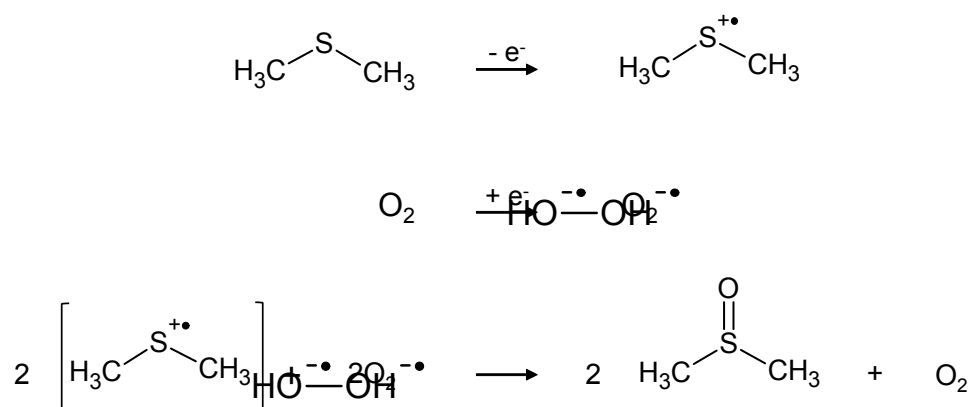


Figure S19. Proposed reaction mechanism at the anode and cathode for the oxidation of DMS.

References

- [1] G. Eda, H. Yamaguchi, D. Voiry, T. Fujita, M. Chen, M. Chhowalla, *Nano Lett.* **2011**, *11*, 5111–5116.
- [2] V. V. Pavlishchuk, A. W. Addison, *Inorganica Chimica Acta* **2000**, *298*, 97–102.
- [3] M. Calandra, *Phys. Rev. B* **2013**, *88*, 245428.
- [4] C. L. Green, A. Kucernak, *J. Phys. Chem. B* **2002**, *106*, 1036–1047.
- [5] M. Calandra, *Phys. Rev. B* **2013**, *88*, 245428.
- [6] G. Kresse, J. Furthmüller, *Phys. Rev. B* **1996**, *54*, 11169–11186.
- [7] G. Kresse, J. Furthmüller, *Computational Materials Science* **1996**, *6*, 15–50.
- [8] J. P. Perdew, K. Burke, M. Ernzerhof, *Phys. Rev. Lett.* **1996**, *77*, 3865–3868.
- [9] S. Grimme, J. Antony, S. Ehrlich, H. Krieg, *J. Chem. Phys.* **2010**, *132*, 154104.
- [10] G. Henkelman, A. Arnaldsson, H. Jónsson, *Computational Materials Science* **2006**, *36*, 354–360.
- [11] L. Li, Z. Qin, L. Ries, S. Hong, T. Michel, J. Yang, C. Salameh, M. Bechelany, P. Miele, D. Kaplan, M. Chhowalla, D. Voiry, *ACS Nano* **2019**, *13*, 6824–6834.

Author contributions

D.V. conceived the idea, designed the experiments and wrote the manuscript. L.M. and K.Q. synthesized the materials and performed the electrocatalytic measurements with Z.Q.. K.Q.

analyzed and discussed the results with D.V.. E.P. carried out the NMR measurements. D.C. performed the SEM observations of the samples. EPR and XPS analyses were carried out by C.R. and V.F. respectively. H.E.M. performed the UPD measurements with L.M.. P.M. and D.K. discussed the results with D.V.. N.O. performed the numerical simulation and discussed the results with D.V. and M.C.. All of the authors edited the manuscript before submission.